Polyhedron 28 (2009) 3331–3339

Contents lists available at ScienceDirect

Polyhedron

journal homepage: www.elsevier.com/locate/poly

pH-Specific synthetic chemistry, and spectroscopic, structural, electrochemical and magnetic susceptibility studies in binary Ni(II)-(carboxy)phosphonate systems

M. Menelaou [a,*], M. Dakanali [b], C.P. Raptopoulou [c], C. Drouza [d], N. Lalioti [e], A. Salifoglou [a]

[a] Department of Chemical Engineering, Aristotle University of Thessaloniki, Thessaloniki 54124, Greece
[b] Department of Chemistry, University of Crete, Heraklion 71409, Greece
[c] Institute of Materials Science, NCSR "Demokritos", Aghia Paraskevi 15310, Attiki, Greece
[d] Department of Agricultural Production and Food Science and Technology, Cyprus University of Technology, Limassol 3603, Cyprus
[e] Department of Chemistry, University of Patras, Patras 26500, Greece

ARTICLE INFO

Article history:
Available online 18 July 2009

This contribution is dedicated to Dr. Aris Terzis on the occasion of his retirement.

Keywords:
pH-Specific synthesis
Ni(II)-(carboxy)phosphonate species
Binary interactions
X-ray structure
Magnetic susceptibility

ABSTRACT

Nickel can play numerous roles in biological systems and in advanced abiotic materials. Supporting the diverse roles of Ni(II) in biological media are, among others, metal ion binding amino acids, their variably phosphorylated forms and/or exogenously administered organophosphonate drug substrates. In an effort to comprehend the aqueous chemistry of interactions between Ni(II) and organophosphonate substrates, research efforts were launched involving the ligands imino bis(methylenephosphonic acid) (H_4IDA2P), $H_2O_3P–CH_2–NH_2^+–CH_2–PO_3H^-$, and *N*-(phosphonomethyl)glycine (glyphosate–H_3IDAP), $HOOC–CH_2–NH_2^+–CH_2–PO_3H^-$. pH-Specific reactions of Ni(II) with H_4IDA2P and H_3IDAP led to the isolation of $[Ni(C_2H_8O_6NP_2)_2(H_2O)_2]$ (**1**) and $[Ni(OOC–CH_2–NH–CH_2–PO_3H)_2]\cdot[Ni(H_2O)_6]\cdot 3.3H_2O$ (**2**), respectively. Compound **1** was characterized by analytical, spectroscopic techniques (UV–Vis, FT-IR), cyclic voltammetry, magnetic susceptibility measurements and X-ray crystallography. Compound **2** was characterized by elemental analysis, FT-IR spectroscopy, and X-ray crystallography. The structures of **1** and **2** reveal mononuclear octahedral Ni(II) assemblies bound by H_3IDA2P^- and water (**1**), and glyphosate ($HIDAP^{2-}$) and water molecules (**2**), respectively. Magnetic susceptibility studies on **1** support the presence of high-spin octahedral Ni(II) in an oxygen environment, consistent with X-ray crystallography. The collective physicochemical features of the discrete Ni(II) assemblies in both species (a) shed light on aqueous binary Ni(II)–phosphoderivative interactions potentially influencing cellular physiology or toxicity, and (b) define the fundamental properties essential for the employment of such species in advanced materials synthesis and applications.

1. Introduction

Nickel is an important transition metal ion present in various living organisms (bacteria, plants and mammals) as well as abiotic systems. In the abiotic world, Ni(II) can be employed in various applications, reflecting its physical and chemical properties, including catalysis [1], electroplating [2], advanced corrosion-resistant materials [3], and elsewhere. In biological systems, numerous studies have been carried out aiming at delineating the involvement of nickel in proteins and enzymes. Nickel transport and storage, regulation, as well as maturation of nickel metalloenzymes are among the most studied processes. In such processes, Ni(II) can act as a metal cofactor, playing an important role in carbon cycling, with characteristic macromolecules being carbon monoxide dehydrogenase (CODH) and acetyl-CoA synthase (ACS). Other functionally outstanding (bio)systems containing Ni(II) ions include urease as well as many but not all hydrogenases [4].

In all (bio)systems, the interaction of Ni(II) with variable nature substrates is crucial in promoting chemistries relevant to metal ionic function at the cellular or abiotic level. In this regard, research efforts, over the last decades, have focused on understanding the arising interactions of phosphorylated and organophosphonate substrates with transition metal ions, such as Co(II), Ni(II), Cu(II), etc. Albeit not the same as the phosphorylated targets in biological media, organophosphonates present similar forms of substituted organic substrates capable of metal ion binding. Moreover, due to their versatile coordination chemistry with a plethora of metal ions, organophosphonates have been associated with the synthesis of variable nuclearity [5–7] and linear one-dimensional compounds [8] as well as layered metal organophosphonates [9,10]. The resulting materials have been found to exhibit interesting reactivity properties rendering them useful in applied fields such as catalysis, ion exchange, intercalation chemistry, film preparation with optical properties, and others [11–15]. More recently,

* Corresponding author. Tel.: +30 2310 994 243; fax: +30 2310 996 196.
E-mail address: melitacy@yahoo.com (M. Menelaou).

0277-5387/$ - see front matter © 2009 Elsevier Ltd. All rights reserved.
doi:10.1016/j.poly.2009.05.084

organophosphonate substrates and especially bis(phosphonate) substrates that represent a useful class of drugs, have been employed in the treatment of bone diseases (Paget's disease of bone, myeloma) [16,17]. The biological benefit of organophosphonate moieties has emerged primarily because of their influence on calcium metabolism and its availability.

On the basis of the above views, interactions arising between organophosphonate binders and metal ions such as Ni(II), are expected to promote metal ion solubilization and influence metallo(bio)chemical processes. Two representative low molecular mass organophosphonic acids are: (a) imino bis(methylenephosphonic acid) (H_4IDA2P), and (b) *N*-(phosphonomethyl) glycine (glyphosate, H_3IDAP). The first organophosphonate substrate H_4IDA2P acts as a binder with two very important features: (a) it contains two phosphonate moieties, known to promote metal ion binding, and (b) it contains one imino group. Glyphosate, on the other hand, is a well-known herbicide first introduced in 1974 under the trade name "Roundup". It is one of the very few biodegradable commercial herbicides used to kill weeds. It is degraded in the soil to the non-toxic products CO_2, NH_3 and PO_4^{3-} within a few days. As in the case of H_4IDA2P, glyphosate (H_3IDAP) exists in a zwitterionic form. Glyphosate possesses three binding sites capable of coordinating metal ions such as Ni(II): (a) a carboxylate moiety, (b) a phosphonate moiety, and (c) an imino moiety. Complexes arising from interactions of glyphosate with metal ions are expected to exhibit a variety of structural attributes including five-membered rings, bestowing stability to the isolated species. The use of a diphosphonate and a (carboxy)phosphonate ligand respectively, exemplifies structural attributes of various phosphorylated analogs of amino acids and organophosphonate-containing drugs. In both cases, it is important to point out the paucity of structurally characterized complexes of organophosphonates with Ni(II) in aqueous media.

Poised to understand the underlying principles of the aqueous chemical reactivity of Ni(II) toward organophosphonate ligands, variably mimicking phosphorylated and phosphonate species in cellular media, the binary systems of Ni(II) with the aforementioned substrates were investigated. Herein, we report on the pH-specific synthesis, isolation and characterization of two new binary Ni(II)–organophosphonate complexes with distinct properties (a) reflecting the nature of interactions involved in binary species of the corresponding aqueous speciation schemes, (b) exemplifying the solid state and solution features potentially relating to the aqueous speciation of Ni(II) with phospho-substituted ligands of biological relevance, seeking to contribute to physiology and/or toxicity, and (c) projecting physicochemical properties akin to Ni(II)–phosphonate materials.

2. Experimental

2.1. Materials and methods

All experiments were carried out in aqueous media under aerobic conditions. Nanopure quality water was used for all reactions. $Ni(NO_3)_2{\cdot}6H_2O$ was purchased from Carlo Erba, and imino bis(methylphosphonic acid), (H_4IDA2P) from Fluka. Ammonia, KOH and NaOH were also supplied by Fluka. Glyphosate (H_3IDAP) was purchased from Aldrich.

2.2. Physical measurements

FT-IR spectra were recorded on a Perkin Elmer 1760X FT-infrared spectrometer. UV–Vis measurements were carried out on a Hitachi U2001 spectrophotometer in the range from 190 to 1000 nm. A ThermoFinnigan Flash EA 1112 CHNS elemental analyzer was used for the simultaneous determination of carbon, hydrogen and nitrogen (%). The analyzer is based on the dynamic flash combustion of the sample (at 1800 °C) followed by reduction, trapping, complete GC separation and detection of the products. The instrument is (a) fully automated and controlled by PC via the Eager 300 dedicated software, and (b) capable of handling solid, liquid or gaseous substances.

A TA Instruments, model Q 600, system was used to run the simultaneous TGA-DTG experiments. The employed heating rate was 10 °C/min. The instrument mass precision is 0.1 μg. About 20 mg of sample was placed in an open alumina sample pan for each experiment. High purity air (80/20 in N_2/O_2) was used at a constant flow rate of 100 mL/min, depending on the conditions required for running the experiment(s). During the experiments, the sample weight loss and rate of weight loss were recorded continuously under dynamic conditions, as a function of time or temperature, in the range 30–1010 °C. Prior to activating the heating routine program, the entire system was purged with the appropriate inert gas for 10 min, at a rate of 400 mL/min, to ensure that the desired environment had been established.

Magnetic susceptibility data were collected on powdered samples of **1** with a Quantum Design SQUID susceptometer in the 2–300 K temperature range, under various applied magnetic fields. Magnetization measurements were carried out at three different temperatures in the field range 0–5 T.

Electrochemical measurements were carried out with a model PGSTAT30 potensiostat-galvanostat from Autolab Electrochemical Instruments. The entire system was under computer control and supported by the appropriate computer software GPES, running on Windows XP. The employed electrochemical cell had platinum (disk) working and auxiliary (wire) electrodes. An Ag/AgCl electrode was used as reference electrode. Thus, the derived potentials in the cyclic voltammetric measurements are referenced to that electrode. The water used in the electrochemical measurements was of nano-pure quality. KNO_3 was used as a supporting electrolyte. Normal concentrations used were 1–6 mM in electroanalyte and 0.1 M in supporting electrolyte. Purified argon was used to purge the solutions prior to the electrochemical measurements. Derived $E_{1/2}$ values are reported versus Ag/AgCl electrode.

2.3. Synthesis of complex $[Ni(C_2H_8O_6NP_2)_2(H_2O)_2]$ (**1**)

(a) A sample of 0.50 g of $Ni(NO_3)_2{\cdot}6H_2O$, (1.7 mmol) and 0.35 g (1.7 mmol) of imino-bis(methylenephosphonic acid) were dissolved in nano-pure water. The pH of the resulting solution was raised to 3 with 0.1 M aqueous ammonia. The derived reaction mixture was stirred at room temperature overnight. On the following morning, the solution was clear and its color was green. Subsequently, the reaction solution was filtered and allowed to stand at room temperature. After a period of several weeks green needle-like crystals grew out of the solution by slow evaporation. The crystalline material was collected by filtration and dried in vacuo. Yield: 0.56 g (~66%). *Anal.* Calc. for **1**, $[Ni(C_2H_8O_6NP_2)_2(H_2O)_2]$ ($C_4H_{20}O_{14}N_2P_4Ni$, MW = 502.81): C, 9.54; H, 3.98; N, 5.57. Found: C, 9.68; H, 4.03; N, 5.64%.

(b) The same reaction was run in the presence of NaOH or KOH, affording morphologically identical green needle-like crystals. The FT-IR spectrum of the crystals and the X-ray unit cell determination of one of the isolated single crystals identified the material as complex **1**.

(c) The same reaction as in (a) was also run with a metal to ligand stoichiometry of 1:2. In this case, green crystalline material was also isolated. FT-IR spectroscopy in combination with X-ray crystallography identified the isolated material as complex **1**.

2.4. Synthesis of complex [Ni(OOC–CH2–NH–CH2–PO3H)2]·[Ni(H2O)6]·3.3H2O (2)

(a) A sample of 0.23 g of $Ni(NO_3)_2{\cdot}6H_2O$ (0.79 mmol) and 0.26 g (1.5 mmol) of *N*-(phosphonomethyl) glycine (glyphosate) were dissolved in nano-pure water. The pH of the resulting solution was raised to 4 with 0.1 M NaOH. The derived reaction mixture was stirred at room temperature. On the following morning, the solution was clear and its color was blue. Subsequently, ethanol was added and the reaction mixture was placed at 4 °C. A few weeks later, bluish crystals appeared at the bottom of the flask. The crystals were isolated by filtration and dried in vacuo. The yield was 0.75 g (~77%). *Anal.* Calc. for **2**, $[Ni(OOC{-}CH_2{-}NH{-}CH_2{-}PO_3H)_2]{\cdot}[Ni(H_2O)_6]{\cdot}3.3H_2O$ ($C_6H_{30.6}O_{19.3}N_2P_2Ni_2$, MW = 619.08): C, 11.63; H, 4.94; N, 4.52. Found: C, 11.89; H, 5.25; N, 4.34%.

(b) A similar reaction as in (a) was carried out using aqueous ammonia to raise the pH. Blue crystalline material appeared at the bottom of the reaction flask. FT-IR spectroscopy in combination with the X-ray determination of the unit cell of a single crystal identified the isolated crystals as complex **2**.

2.5. X-ray crystal structure determination

X-ray quality crystals of compound **1** were grown from aqueous reaction mixtures upon slow evaporation. A single crystal with dimensions 0.15 × 0.09 × 0.05 mm was mounted on the tip of a glass fiber with epoxy glue. The crystal was mounted on an Xcalibur Oxford Diffractometer equipped with a Sapphire 3 CCD detector and a 4-cycle Kappa geometry goniometer, using an enhanced Mo X-ray source and graphite radiation monochromator. Unit cell dimensions for **1** were determined and refined by using the angular settings of all the reflection frames in the range $6.30 < 2\theta < 60.50°$. Relevant crystallographic data appear in Table 1. An analytical absorption correction was applied using CrysAlis RED software. CrysAlis CCD and CrysAlis RED software were used for monitoring data collection and computing data reduction/cell refinement, respectively [18,19]. The structure was solved by direct methods and refined by full-matrix least-squares techniques on F^2 by using SHELXS-97 [20,21]. Special computing molecular graphics incorporated in the WinGX 3.2 interface were used [22]. Further crystallographic details for **1**: $2\theta_{max} = 62.44°$; reflections collected/unique/used, 11 076/2263 [$R_{int} = 0.0669$]/2263; parameters refined, 136; $[\Delta\rho]_{max}/[\Delta\rho]_{min}$ = 0.895/−0.686 e/Å^3; R/R_w (for all data), 0.0291/0.0720. All of the non-H atoms were refined anisotropically. The methylene hydrogen atoms of the phosphonate ligand were introduced at calculated positions as riding on bonded atoms. The remainder of the hydrogen atoms were located by difference Fourier maps and were refined isotropically. Further details on the crystallographic studies as well as atomic displacement parameters are given as Supporting Information in the form of cif files.

X-ray quality crystals of compound **2** were grown from water–ethanol mixtures. A single crystal, with dimensions 0.06 × 0.20 × 0.28 mm was mounted on a Crystal Logic dual-goniometer diffractometer, using graphite monochromated Mo Kα radiation (λ = 0.71073 Å). Unit cell dimensions for **2** were determined and refined by using the angular settings of 25 automatically centered reflections in the range $11.00 < 2\theta < 23.00°$. Crystallographic details are given in Table 1. Intensity data were measured by using θ–2θ scans. Three standard reflections were monitored every 97 reflections, over the course of data collection at 298 K. They showed less than 3% variation and no decay. Lorentz, polarization and psi-scan absorption corrections were applied by using Crystal Logic software. The structure of complex **2** was solved by direct methods using SHELXS-97 [20]. Refinement was achieved by full-matrix least-squares techniques on F^2 with SHELXL-97 [21]. Further crystallographic details for **2**: $2\theta_{max} = 50.00°$; reflections collected/unique/used, 4042/3915 [$R_{int} = 0.0249$]/3915; parameters refined, 381; $[\Delta\rho]_{max}/[\Delta\rho]_{min}$ = 2.023/−0.861 e/Å^3; R/R_w (for all data), 0.0697/0.1645. All hydrogen atoms were located in difference maps and were refined isotropically; no H-atoms for the partially occupied water solvate molecules were included in the refinement. All non-H atoms were refined anisotropically.

Table 1
Summary of crystal, intensity collection and refinement data for compounds $[Ni(C_2H_8O_6NP_2)_2(H_2O)_2]$ (**1**) and $[Ni(OOC\text{-}CH_2\text{-}NH\text{-}CH_2\text{-}PO_3H)_2]{\cdot}[Ni(H_2O)_6]{\cdot}3.3H_2O$ (**2**).

	1	**2**
Chemical formula	$C_4H_{20}N_2O_{14}P_4Ni$	$C_6H_{30.6}O_{19.3}N_2P_2Ni_2$
Formula weight	502.81	619.08
Temperature (K)	100 (2)	298 (1)
Wavelength, λ (Å)	Mo Kα 0.71073	Mo Kα 0.71073
Space group	$P2_1/n$	$P2_1/n$
a (Å)	7.3657(7)	9.138(5)
b (Å)	8.0937(10)	13.352(6)
c (Å)	13.8973(15)	18.382(9)
α (°)	90.00	90.00
β (°)	104.527(9)	94.33(2)
γ (°)	90.00	90.00
V (Å^3)	802.01(15)	2236.5(18)
Z	2	4
ρ_{calcd}/ρ_{obsd} (g/cm^3)	2.082/2.078	1.839/1.831
Absorption coefficient (μ) (mm^{-1})	1.686	1.916
Range of *h*, *k*, *l*	−10 → 10, −10 → 11, −19 → 19	−10 → 10, −15 → 0, −21 → 0
R^a	0.0258[b]	0.0623[b]
$R_w{}^a$	0.0714[b]	0.1559[b]

[a] *R* values are based on *F*'s, R_w values are based on F^2; $R = \frac{\sum ||F_o|-|F_c||}{\sum(|F_o|)}$, $R_w = \sqrt{\sum[w(F_o^2 - F_c^2)^2] / \sum[w(F_o^2)^2]}$.

[b] For 1943 (**1**) and 3456 (**2**) reflections with $I > 2\sigma(I)$.

2.6. Synthesis

The synthesis of compound **1** was pursued through a pH-specific reaction between Ni(II) and imino-bis(methylenephosphonic acid) (H_4IDA2P) in aqueous media. The pH, at which the reaction was developed, was 3. The adjustment of pH was achieved by adding aqueous ammonia (NaOH or KOH). The stoichiometric reaction leading to the isolation of compound **1** is shown below (Reaction 1):

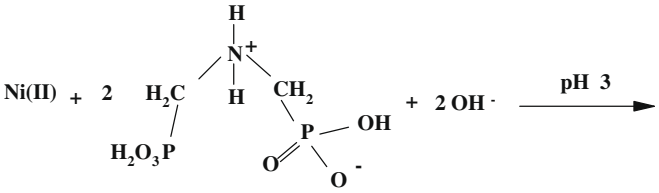

$[Ni(C_2H_8O_6NP_2)_2(H_2O)_2]$

(Reaction1)

Compound **1** was easily isolated in pure crystalline form after several weeks of having the reaction flask stand in the air. Elemental analysis of the isolated green crystalline material suggested the molecular formulation $[Ni(C_2H_8O_6NP_2)_2(H_2O)_2]$ for **1**. It appears that the sole purpose of the employed aqueous base solutions was to adjust the pH of the reaction mixture. No cations arising from the use of such bases were found to be incorporated into the arising lattice of **1**. Further examination of **1** by FT-IR spectroscopy confirmed the presence of the phosphonate moieties bound to Ni(II), thus lending credence to the proposed formulation. Compound **1** is sparingly soluble in water, but it is insoluble in organic solvents, such as acetonitrile, chlorinated solvents ($CHCl_3$, CH_2Cl_2), toluene and DMF.

The pH-specific synthesis of compound **2** was achieved through a similar reaction to that of compound **1**. In the synthesis of **2**, employing the carboxy-phosphonate ligand *N*-(phosphonomethyl) glycine in aqueous media, the pH of the reaction mixture was 4. The adjustment of pH was achieved by adding aqueous NaOH (or ammonia). The stoichiometric reaction leading to the isolation of **2** is shown below (Reaction 2):

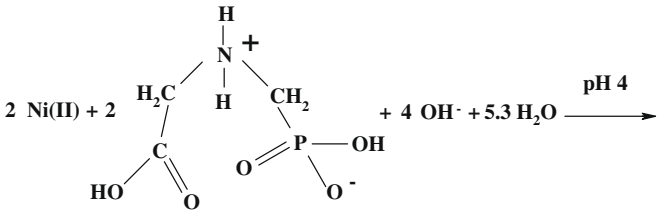

(Reaction2)

Elemental analysis of the isolated blue crystalline material suggested the molecular formulation $[Ni(OOC–CH_2–NH–CH_2–PO_3H)_2]·[Ni(H_2O)_6]·3.3H_2O$. It appears that employment of the two separate base solutions used in the synthesis contributed solely to the adjustment of the reaction mixture pH, in view of the fact that Na^+ and NH_4^+ ions were not incorporated in the ultimate lattice of **2**. Further examination of **2** by FT-IR spectroscopy confirmed the presence of phosphonate and carboxylate moieties bound to Ni(II), thus supporting the proposed formulation. Compound **2** is insoluble in water as well as in organic solvents, such as acetonitrile, chlorinated solvents ($CHCl_3$, CH_2Cl_2), toluene and DMF.

2.7. Description of the structures

2.7.1. Compound $[Ni(C_2H_8O_6NP_2)_2(H_2O)_2]$ (1)

The X-ray crystal structure of **1** reveals the presence of discrete species in a molecular type of lattice. The crystal structure diagram of **1** is shown in Fig. 1A, while a packing view of the same complex is provided in Fig. 2A. A list of selected bond distances and angles for **1** is given in Table 2. Complex **1** crystallizes in the monoclinic space group $P2_1/n$ with two molecules per unit cell. The structure shows a mononuclear assembly of Ni(II) bound to two H_3IDA2P^- ligands. In particular, there are two different ligands bound to Ni(II), namely imino bis(methylenephosphonate) ($^-HO_3P–CH_2–NH_2^+–CH_2–PO_3H^-$ = H_3IDA2P^-) and water. The two H_3IDA2P^- ligands in the coordination sphere of Ni(II) are singly deprotonated with the deprotonation site being the hydroxide group of the phosphonate moiety. The second hydroxide group of each phosphonate moiety remains in the protonated form. In this respect, each phosphonate group acts as a monodentate ligand. Finally, two water molecules lie in the equatorial plane of the octahedral metal ion Ni(II).

Analogous cases of bound bis(phosphonate) metal complexes had been previously observed in the case of Co(II) and Mn(II). Specifically, the characterized complexes $[Co(C_2H_8O_6NP_2)_2(H_2O)_2]$ (**3**) [23] and $[Mn(C_2H_8O_6NP_2)_2(H_2O)_2]$ (**4**) [24] exhibit a coordination environment similar to that of Ni(II) generated by two H_3IDA2P^- ligands and two water molecules. A different coordination environment, however, is present in the case of other metal complexes with H_4IDA2P: $Cu[NH(CH_2PO_3H)_2]$ (**5**) [25], $Pb_2[NH(CH_2PO_3)_2]·2H_2O$ (**6**) [26], $Mn[NH_2(CH_2PO_3H)(CH_2PO_3)]·H_2O$ (**7**) [25], $Cu_3[NH_2(CH_2PO_3)_2]_2$ (**8**) [24], $Co_3[NH_2(CH_2PO_3)_2]_2$ (**9**) [24], and $\{Mn[NH(CH_2PO_3H)_2](H_2O)_2\}_2·\{Mn(C_4O_4)(H_2O)_4\}·(C_4H_2O_4)$ (**10**) [27].

The Ni–O bond distances (2.037(1)–2.093(1) Å) in **1** compare favorably with those observed in the crystal structure of complexes $(NH_3CH_2CH_2NH_3)·\{Ni(O_2CCH_2N(CH_2PO_3H)_2](H_2O)_2\}_2$ (2.028(6)–2.097(6) Å) (**11**) [28], $Ni[HO_3PCH_2N(CH_3)CH_2CH_2N(CH_3)CH_2PO_3H](H_2O)_2$ (2.052(4)–2.074(4) Å) (**12**) [29], $[C_{30}H_{50}N_8Ni_2O_2(H_2O)_2]·(ClO_4)_2·CH_3OH·3H_2O$ (2.041(2)–2.141(2) Å) (**13**) [30], and $[Ni(pyr)(H_2O)_4]·[Ni(C_5H_7NO_7P)_2(pyr)(H_2O)_2]·2H_2O$ (2.038(2)–2.110(2) Å) (**14**) [31].

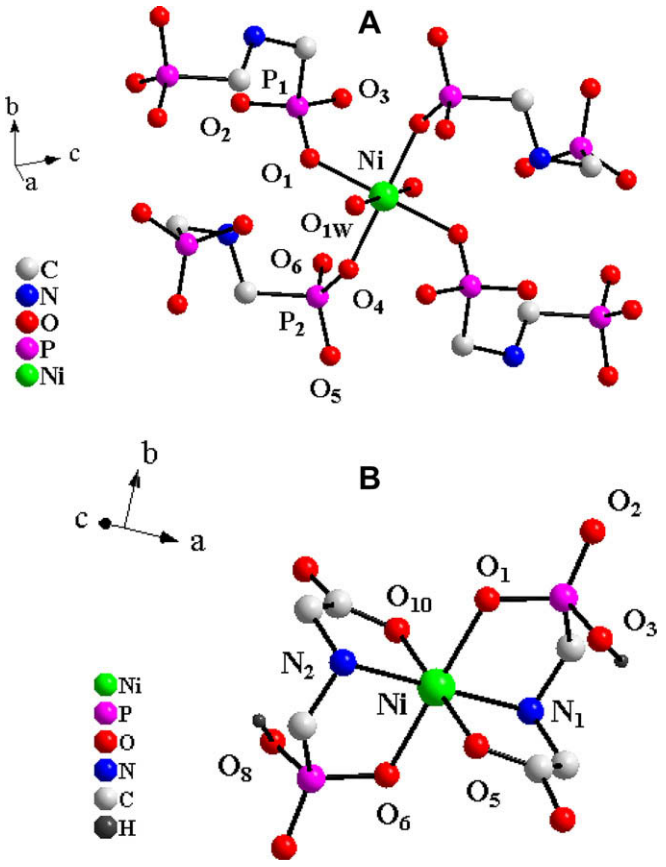

Fig. 1. (A) Crystal structure of $[Ni(C_2H_8O_6NP_2)_2(H_2O)_2]$ (**1**). (B) Partially labeled plot of the anion in **2** with thermal ellipsoids at the 30% probability level.

The angles within the equatorial plane defined by O(4), O(4)′, O(1w) and O(1w)′ are in the range 87.11(5)–92.89(5)°, and hence fairly close to the ideal octahedral angle of 90°. A similar angle variation is observed between the axial donor atoms O(1) and O(1)′ and those in the equatorial plane (range: 86.46(4)–93.54(4)°). The aforementioned angle values are similar to those observed in (**3**)–(**10**) as well as in complexes arisen through interactions of other divalent metals with a diphosphonate ligand similar to H_4IDA2P, i.e. $[Cu(HO_3PC(CH_3)(OH)PO_3H)_2]^{2-}$ (84.7–95.3° and 87.8–92.2°, respectively) [32] and $[Zn(HO_3PC(CH_3)(OH)PO_3H)_2]^{2-}$ (85.0–95.0° and 88.6–91.4°, respectively) [33].

The mode of coordination of the H_3IDA2P^- ligand to Ni(II) in **1** is monodentate. The exact same behavior is observed in the case of the divalent metal ions Co(II) and Mn(II). In the free form, H_4IDA2P consists of two terminal phosphonate groups, both of them capable of binding to Ni(II). However, in the work presented here, the terminal phosphonate group is coordinated to an adjacent Ni(II) ion, which in turn is surrounded by the same type of ligands in an octahedral environment. Finally, the four H_3IDA2P^- binders surrounding the central metal ion Ni(II), are also bound to four other Ni(II) ions due to the presence of the second phosphonate group in each H_4IDA2P molecule. In this sense, saturation of the coordination sites in contiguous octahedral Ni(II) ions extends to infinity, thereby giving rise to the molecular lattice in **1**.

An interesting attribute of the iminodiphosphonate ligand is the presence of a protonated central imino group, reflecting the zwitterionic form of the ligand. Hence, the interaction of the H_3IDA2P^-

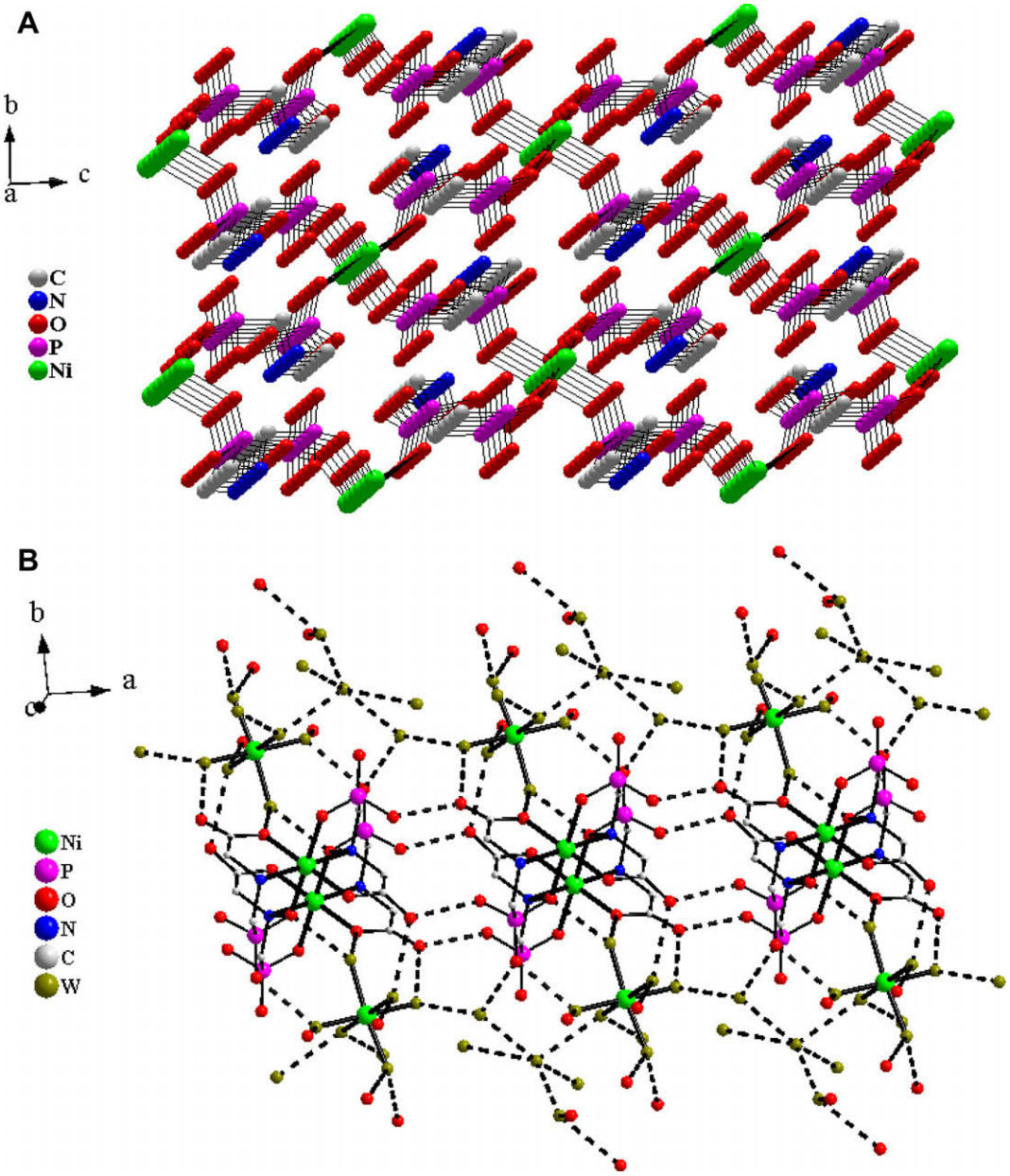

Fig. 2. (A) Packing view of complex **1** in the *bc* plane. (B) Section of the 3D structure of **2** reflecting hydrogen bonding interactions. Water molecules (Ni-bound and free) in the figure are represented as W.

ligand with Ni(II), affording complex **1**, denotes the presence of two singly deprotonated phosphonate groups and a singly protonated imino group. As a result, the overall charge of the iminodiphosphonate ligand coordinated to Ni(II) ion is 1−. Two of these ligands need to balance the overall zero charge of the isolated species. The two additional H_3IDA2P^- ligands coordinated to Ni(II) do not contribute to the overall charge, as they originate in an adjacent mononuclear Ni(II) site and complete the octahedral coordination sphere of Ni(II). The remaining two coordination sites of Ni(II) ion are occupied by two water molecules.

2.7.2. Compound $[Ni(OOC–CH_2–NH–CH_2–PO_3H)_2]·[Ni(H_2O)_6]·3.3H_2O$ (**2**)

Complex **2** crystallizes in the monoclinic space group $P2_1/n$ with four molecules per unit cell. The lattice of **2** consists of discrete mononuclear cations and anions. A list of selected bond distances and angles for **2** is given in Table 2. In the first mononuclear unit, the six coordination sites of Ni(II) (Ni(1)) are occupied by two glyphosate ligands (Fig. 1B). Each glyphosate ligand bound to Ni(II) ion acts as a chelator with a 2− charge ($HIDAP^{2-}$), since the two terminal sites of the glyphosate ligand are deprotonated, i.e. the carboxylate and phosphonate moieties. The second hydroxide moiety of the phosphonate group remains protonated. The imino nitrogen of the bound glyphosate ligand is not protonated as in the case of the H_3IDA2P^- ligand in **1**. As a result, it actively participates in the coordination of the $HIDAP^{2-}$ ligand to the central Ni(II) ion. To this end, in each bound glyphosate two five-membered chelate rings form, defined by Ni–N–C–P–O and Ni–N–C–C–O, respectively, which provide stability to the isolated complex **2**. The two five-membered rings defined by Ni–N–C–P–O adopt the stable envelope configuration with atoms C(4) and C(1) displaced ~0.60 Å out of the best mean plane of the remaining four atoms. In the case of the five-membered rings defined by Ni–N–C–C–O, the out-of-plane atoms are C(2) and C(5), displaced at 0.31 and 0.25 Å, respectively, out of the best mean plane of the remaining four atoms. The negative charge of the first mononuclear unit is counterbalanced

Table 2
Bond lengths [Å] and angles [°] for $[Ni_2(C_2H_8O_6NP_2)_2(H_2O)_2]$ (**1**) and $[Ni(OOC–CH_2–NH–CH_2–PO_3H)_2]\cdot[Ni(H_2O)_6]\cdot 3.3H_2O$ (**2**).

1		2	
Distances			
Ni(1)–O(4)	2.037(1)	Ni(1)–O(1)	2.132(4)
Ni(1)–O(1 W)	2.048(1)	Ni(1)–O(5)	2.059(4)
Ni(1)–O(1)	2.093(1)	Ni(1)–O(6)	2.113(4)
O(2)–P(1)	1.510(1)	Ni(1)–N(1)	2.092(5)
O(5)–P(2)	1.513(1)	Ni(1)–N(2)	2.097(4)
O(4)–P(2)	1.494(1)	Ni(1)–O(10)	2.049(4)
O(3)–P(1)	1.560(1)		
O(1)–P(1)	1.507(1)		
O(6)–P(2)	1.567(1)		
N(1)–C(1)	1.501(2)		
N(1)–C(2)	1.501(2)		
Angles			
O(4)′–Ni(1)–O(4)	180.00(6)	O(10)–Ni(1)–O(5)	179.2(2)
O(4)′–Ni(1)–O(1W)′	87.11(5)	O(10)–Ni(1)–N(1)	97.4(2)
O(4)–Ni(1)–O(1W)′	92.89(5)	O(5)–Ni(1)–N(1)	82.2(2)
O(4)–Ni(1)–O(1W)	87.11(5)	O(10)–Ni(1)–N(2)	82.4(2)
O(1W)′–Ni(1)–O(1W)	180.00(5)	O(5)–Ni(1)–N(2)	98.0(2)
O(4)′–Ni(1)–O(1)′	88.72(4)	N(1)–Ni(1)–N(2)	179.5(2)
O(4)–Ni(1)–O(1)′	91.28(4)	O(10)–Ni(1)–O(6)	90.1(2)
O(1W)′–Ni(1)–O(1)′	86.46(4)	O(5)–Ni(1)–O(6)	89.2(2)
O(1W)–Ni(1)–O(1)′	93.54(4)	N(1)–Ni(1)–O(6)	93.9(2)
O(4)′–Ni(1)–O(1)	91.28(4)	N(2)–Ni(1)–O(6)	86.6(2)
O(4)–Ni(1)–O(1)	88.72(4)	O(10)–Ni(1)–O(1)	90.6(2)
O(1W)′–Ni(1)–O(1)	93.54(4)	O(5)–Ni(1)–O(1)	90.1(2)
O(1W)–Ni(1)–O(1)	86.46(4)	N(1)–Ni(1)–O(1)	86.0(2)
O(1)′–Ni(1)–O(1)	180.00(3)	N(2)–Ni(1)–O(1)	93.5(2)
P(2)–O(4)–Ni(1)	140.06(7)	O(6)–Ni(1)–O(1)	179.2(2)

Symmetry operations for **1** and **2**: (i) x, y, z; (ii) $-x+1/2,\ y+1/2,\ -z+½$; (iii) $-x, -y, -z$ and (iv) $x-1/2, -y-1/2, z-1/2$.

by the positive charge of the second mononuclear unit, which is the well-known hexa-aqua Ni(II) ion $[Ni(H_2O)_6]^{2+}$ (Ni(2)). Ni(2) is coordinated to six water molecules in an octahedral fashion, displaying a 2+ charge.

Finally, it is worth re-emphasizing the presence of the hexa-aqua Ni(II) ion, $[Ni(H_2O)_6]^{2+}$, in the lattice of complex **2**. This mononuclear dicationic unit is not unlikely to appear in a crystal lattice. It was observed in the lattice of other Ni(II)-complexes displaying similar ligand coordination modes, including: $[Ni(H_2O)_6][Ni(H_2O)_2(C_4H_2O_4)]\cdot 4H_2O$ (**20**) [34], $[Ni(H_2O)_6][Ni_2(C_{10}H_4O_4N_2)_3]\cdot 5H_2O$ (**21**) [35], $[Ni(H_2O)_6][Ni(C_4H_4O_4S)_2]\cdot 4H_2O$ (**22**) [36] and $[Ni(H_2O)_6][Ni(C_7H_3O_4N)_2(H_2O)_2]$ (**23**) [37].

The Ni(1)–O distances (2.049(4)–2.132(4) Å) in complex **2** are similar to those observed in other Ni(II)–O, N compounds (**11**–**14**). The glyphosate ligand, on the other hand, is coordinated in a variety of coordination modes exemplified in the following complexes reported in the literature: $[Cd(C_3H_6NO_5P)(H_2O)_2]_n$ (**15**) [38], $NaCu[O_2CCH_2NHCH_2PO_3]\cdot 3.5H_2O$ (**16**) [6], $Pb[O_3PCH_2NH_2CH_2COO]$ (**17**) [39] and the trivalent metal ion complexes $Na_3[Co(C_3H_5PNO_5)_2]\cdot 11H_2O$ (**18**) [40] and $[Eu_2(HO_3PCH_2NH_2CH_2CO_2)_2(H_2O)_7(ClO_4)]\cdot 3ClO_4\cdot H_2O$ (**19**) [41]. The lattice structure of **2** is stabilized by an extensive hydrogen bonding pattern (Fig. 2B, Table 3) in a 3D network.

2.8. UV–Vis spectroscopy

The UV–Vis spectrum of **1** was recorded in water (Fig. 3). The spectrum exhibits a major absorption at $\lambda_{max} = 395$ nm ($\varepsilon \sim 2.5\ M^{-1}\ cm^{-1}$) and a distant band around 208 nm ($\varepsilon \sim 25\ M^{-1}\ cm^{-1}$). The remaining absorption features are most likely due to d–d transitions typical for a Ni(II) d^8 octahedral species [42]. The absorption feature around 395 nm ($\varepsilon \sim 2.5\ M^{-1}\ cm^{-1}$) could be tentatively attributed to the $^3A_{2g} \rightarrow {}^3T_{1g}(P)$ transition. The observed multiple structure containing the 656 and 730 nm features, a region normally corresponding to the $^3A_{2g} \rightarrow {}^3T_{1g}(F)$ transition, is in line with literature reports invoking the presence of an ^1E_g state lying so close to $^3T_{1g}$ that extensive mixing takes place. That mixing leads to the observation of a doublet band, where the spin forbidden transition picks up intensity from the spin-allowed transition, thus accounting for the complexity of the spectrum [43]. In the absence of detailed studies no further assignments could be proposed.

Table 3
Hydrogen bonds in **2**.

Interaction	D···A (Å)	H···A (Å)	D–H···A (°)	Symmetry operation
O3–HO3···O9	2.566	1.416	163.9	$1+x, y, z$
O8–HO8···O4	2.600	1.906	163.7	$-1+x, y, z$
N1–HN1···O6	3.114	2.454	172.4	$-x, -y, -z$
W1–Hw1A···O9	2.763	1.805	165.7	$-x, -y, -z$
W1–Hw1B···W7	2.812	2.243	175.7	$1+x, -1+y, z$
W2–Hw2A···O10	2.714	2.002	164.8	$-x, -y, -z$
W2–Hw2B···O6	2.716	1.888	165.5	x, y, z
W3–Hw3A···O7	2.685	1.989	157.6	x, y, z
W3–Hw3B···O3	2.911	2.071	158.0	$0.5-x, -0.5+y, 0.5-z$
W4–Hw4A···O5	2.723	2.071	163.7	$0.5-x, -0.5+y, 0.5-z$
W4–Hw4B···O2	2.657	1.774	131.7	$x, -1+y, z$
W5–Hw5A···O1	2.716	1.970	162.7	$0.5-x, -0.5+y, 0.5-z$
W5–Hw5B···O4	2.869	2.228	161.5	x, y, z
W6–Hw6A···W8	2.761	1.977	173.1	$x, -1+y, z$
W6–Hw6B···W8	2.817	2.021	166.7	$-x, -y, -z$
W7–Hw7A···O7	2.733	2.185	160.3	$x, 1+y, z$
W7–Hw7B···W1	2.812	1.715	152.2	$-1+x, 1+y, z$
W8–Hw8A···W9	2.680	1.603	159.0	x, y, z
W8–Hw8B···W10	3.230	2.179	166.8	$-x, 1-y, -z$
W9–Hw9A···O1	2.845	1.700	161.2	x, y, z
W9–Hw9B···O4	2.862	1.925	170.7	$0.5-x, 0.5+y, 0.5-z$

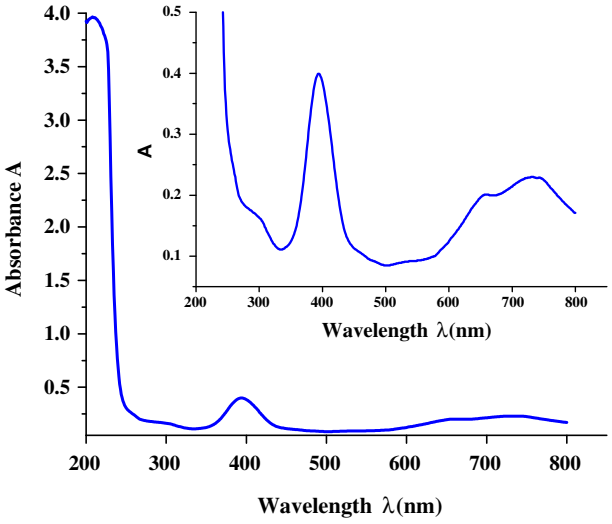

Fig. 3. UV–Vis spectrum of **1** in water.

2.9. FT-IR spectroscopy

The FT-IR spectrum of **1** was recorded in KBr. The spectrum exhibits strong absorptions for the PO_3 groups observed in both the antisymmetric $\nu_{as}(PO_3)$ and symmetric $\nu_s(PO_3)$ vibration regions. Specifically, the antisymmetric stretching vibrations appear in the range between 1090 and 980 cm^{-1}, whereas the symmetric stretching vibrations appear in the range 970–920 cm^{-1}. The frequencies for the aforementioned stretches appear to be shifted to lower values compared to those of free H_4IDA2P acid, indicating changes in the vibrational status of the ligand due to coordination to the Ni(II) ion [23,24].

The FT-IR spectrum for complex **2** in KBr exhibits strong absorptions for the vibrationally active carbonyl moiety of the

carboxylate and PO_3 groups of the glyphosate ligand in both the antisymmetric and symmetric vibration regions. The antisymmetric stretching vibrations $\nu_{as}(COO^-)$ appear in the range from 1600 to 1550 cm^{-1}, whereas the corresponding symmetric stretches $\nu_s(COO^-)$ appear in the range from 1475 to 1385 cm^{-1}. In the same respect, the antisymmetric stretching vibrations $\nu_{as}(PO_3)$ appear in the range from 1209 to 1140 cm^{-1}, whereas the symmetric stretching vibration $\nu_s(PO_3)$ appear in the range from 1074 to 993 cm^{-1}. The frequencies of the various stretches are shifted to lower values compared to those of the free glyphosate binder, due to the coordination of the ligand to the Ni(II) ion [44].

2.10. Thermogravimetric studies

The thermal decomposition of both **1** and **2** was studied by TGA-DTG under an atmosphere of oxygen (see Supplementary data). The TGA diagram shows that an initial process involves the loss of water molecules per formula unit of **1**. The release of Ni(II)-coordinated water molecules until 285 °C, signifies an exothermic process associated with the specific part of the diagram. The observed weight loss amounts to 9.2%, a value very close to the calculated value of 7.2% based on the molecular formula of **1**. Two additional steps are observed in the thermal decomposition of **1**: (a) the release of water molecules due to condensation of the hydrogen phosphonate groups, and (b) the decomposition of the organic moiety. The total weight loss of complex **1** is close to 60.0% and is reached at approximately 1000 °C.

In much the same fashion, the TGA diagram of **2** shows an initial process reflecting the loss of water molecules. The release of all water molecules up until ~300 °C, signifies an exothermic process associated with the specific part of the diagram. The observed weight loss amounts to 28.2%, a value very close to the calculated value of 27.0% based on the molecular formula of the title complex. Two additional steps are observed owing to (a) the carboxylate and phosphonate moieties, and (b) the decomposition of the organic moiety in **2**. The total weight loss due to the decomposition of all the organic composition of **2** is 45.7% and is reached at approximately 935 °C, signifying an endothermic process. The small number of observed TGA peaks reflects simple mechanisms of decomposition for complex **2**.

2.11. Cyclic voltammetry

The cyclic voltammetry of complex **1** was studied in aqueous solutions, in the presence of KNO_3 as a supporting electrolyte (Fig. 4). The cyclic voltammogram projects a well-defined electrochemical behavior, with a pronounced chemically reversible process reflecting: (a) a reduction wave at E_{pc} 0.436 V, and (b) an oxidation wave at E_{pa} 0.616 V, and $E_{1/2}$ 526 mV ($i_{pc}/\{(v)^{1/2}C\}$ constant and $i_{pa}/i_{pc} = 1$). This behavior reflects a process involving the Ni(II)/Ni(III) redox couple. Attempts to pursue the redox chemistry of complex **1** at such high redox potentials are currently ongoing.

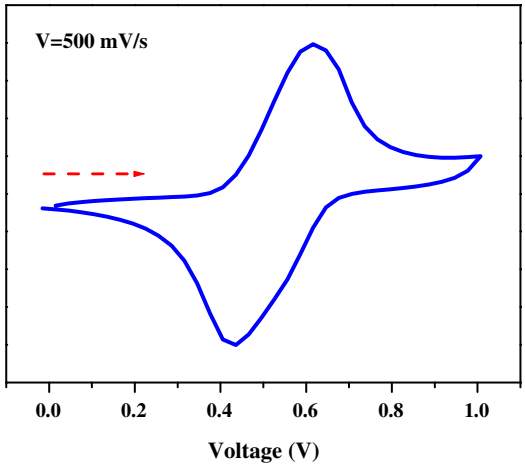

Fig. 4. Cyclic voltammetry of complex **1** in aqueous solutions (scan rate 500 mV/s).

2.12. Magnetic susceptibility studies

Magnetic susceptibility measurements were carried out at different magnetic fields in the temperature range 2–300 K. The temperature dependence of $\chi_M T$ (χ_M being the magnetic susceptibility for one Ni(II) ion) for complex **1** is shown in Fig. 5 (open stars). The $\chi_M T$ value is 1.42 emu mol^{-1} K at 300 K and until 10 K there is a smooth linear decrease. Below that temperature and down to 2 K, a more pronounced decrease occurs reaching the value of 0.8 emu mol^{-1} K. The shape of this curve is characteristic of the occurrence of large zero field effects along with the temperature independent paramagnetism (TIP) effect. The latter effect leads to a linear temperature dependence of the susceptibility data. The susceptibility data were fitted by the following equation:

$$H = D\left[S_z^2 - \frac{1}{3}S(S+1)\right] + E(S_x^2 - S_y^2) + g_z\mu_B H_z S_z + g_x\mu_B H_x S_x + g_y\mu_B H_y S_y \quad (1)$$

where an isotropic g-value was used. The best fit (solid line in Fig. 5) is given by the parameters $D = 4.3(2)$ cm^{-1} and $g = 2.3(1)$, TIP = 9.8×10^{-4}. In the inset of the figure, simulations of the susceptibility function are shown for different values of the D parameter, where the g and TIP values were those obtained from the fitting procedure.

2.13. Magnetization studies

The isothermal magnetization curve at $T = 1.8$ K, in the applied field 0–5 T, is shown in Fig. 6. The curves for the increasing and decreasing fields are identical. The data were fitted using (Eq. (1)) and the best fit (solid line in Fig. 6) is given by the parameters of $D = 3.8(1)$ cm^{-1}, $g = 2.3(1)$. The latter are very close to the values

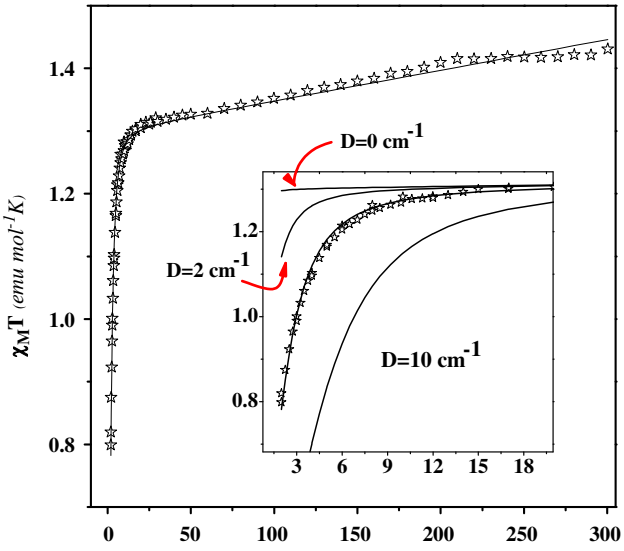

Fig. 5. Temperature dependence of the susceptibility data in the form of $\chi_M T$ vs. T (solid stars) and the fitting results using the theoretical formula discussed in the text (solid line). In the inset simulations of the susceptibility function are shown, in the form of $\chi_M T$ vs. T, for different values of the D parameter.

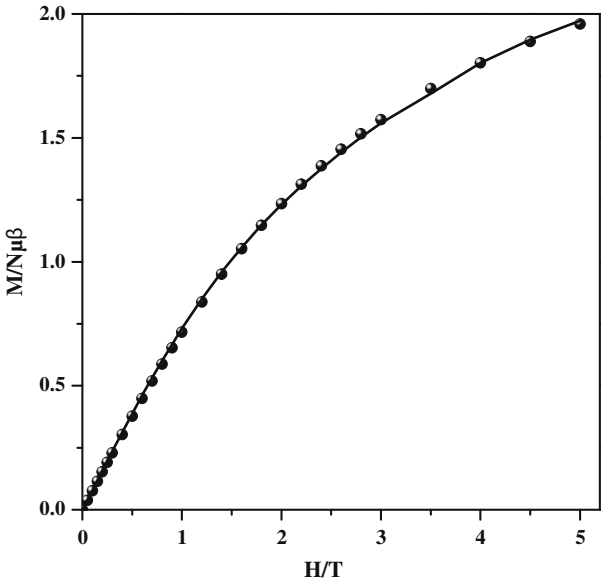

Fig. 6. Magnetization measurements, in the form of $M/N_{\mu\beta}$ vs. H/T, in the field range 0–5 T and at temperature $T = 2$ K, and fitting results using the theoretical formula discussed in the text (solid line).

obtained from the susceptibility study, thus verifying the large zero-field character of the system.

3. Discussion

3.1. The aqueous binary Ni(II)–organophosphonate chemistry

The interaction of two organophosphonate ligands with the divalent metal ion Ni(II), at specific pH values in aqueous media, led to the isolation of two compounds (**1** and **2**). The two ligands employed in these interactions exhibit a zwitterionic form in the free state, i.e. $H_2O_3P–CH_2–NH_2^+–CH_2–PO_3H^-$ and $HOOC–CH_2–NH_2^+–CH_2–PO_3H^-$. This zwitterionic form is essential to the developing synthetic chemistry with Ni(II). In both binary Ni(II)–phosphonate systems, a number of factors appeared to play a role in the isolation of **1** and **2**: (a) the pH of the employed reaction mixture. The acidic reaction conditions in both cases facilitated the formation of the crystalline compounds. Raising the pH of the reaction mixture resulted in the formation of a precipitate of non-crystalline nature in both systems. In the case of the binary Ni(II)–H_4IDA2P system, formation of insoluble precipitate occurred at pH 4, with no dissolution of the precipitate observed at higher pH values. In contrast to that behavior, formation of a precipitate in the second binary system occurred at pH 7. In view of the ostensible pH-dependent behavior of the two binary Ni(II)–organophosphonate systems, it would not be unlikely to consider the existence of the carboxylic moiety in the glyphosate molecule as one of the key factors providing increased solubility to the Ni(II)–glyphosate system compared to the diphosphonate counterpart and (b) the involvement of the alkali solutions in the adjustment of the reaction mixture pH of each binary system investigated. Despite the use of different bases (NaOH, KOH, ammonia) in the binary reaction mixtures, the molecular formulation of the isolated products, as proven by elemental analysis and X-ray crystallography, did not include counter ions originating in those bases. Therefore, the sole use of bases was to adjust the pH and facilitate isolation of the crystalline products **1** and **2**. Moreover, in the case of complex **1**, different molar ratios in the Ni(II)–H_4IDA2P system were employed affording the isolation of **1**. It appears, therefore, that complexes **1** and **2** are stable enough to be isolated under variable reaction conditions. Even though, **1** and **2** are the first isolated products resulting from the interaction of Ni(II) with the two aforementioned phosphonate ligands, the possibility of other Ni(II)-(carboxy)phosphonate species (arising from such specific interactions) being present in solution and currently eluding isolation and characterization, cannot be discounted.

Undoubtedly, the herein described species **1** and **2** project chemical and structural features that emphasize (a) the unique chemistry of phosphonate and mixed carboxy-phosphonate substrates toward Ni(II), and (b) the differentiation of the composition and structure of the derived and ultimately isolated species brought about by the distinct nature of the phosphonate substrates reacting with Ni(II) under the employed conditions. Collectively, therefore, the observed physicochemical behavior of the substrates H_4IDA2P and H_3IDAP influences quite elegantly the nature of binary interactions developing between them and Ni(II). To this end, it would not be unreasonable to envision analogous interactions emerging between that metal ion and corresponding phosphorylated substrates (amino acids, peptides, proteins) and organophosphonate drug substrates in the requisite aqueous speciation of a biological setting. Delving into the exploration of such interactions (a) with low and high molecular mass phospho-derivative biotargets, and (b) at the binary and ternary level, is a challenge of multidisplinary approaches, currently under investigation in the lab.

3.2. Relevance to Ni(II)–organophosphonate materials

Over the last decades, special attention has focused on delineating the reactivity of organophosphonate ligands toward metal ions, such as Ni(II), Co(II), Mn(II), etc. Materials arising from such interactions are employed in a plethora of applications, including catalysis and intercalation chemistry. In this regard, the nature of the organophosphonate binders is crucial in the isolation of metal–ligand frameworks with well-defined properties. Substrates containing one phosphonate group [45,46], such as glyphosate, or various diphosphonic acids [47,48], such as $H_2O_3P–R–PO_3H_2$ (R=alkyl, phenyl, alkylimino, benzylimino, etc.) under diverse reaction conditions are likely to afford new interesting materials with variable physicochemical properties reflected into the size of the employed binder, the shape, the complexity, the nature of the terminal groups, and their chemical reactivity. Under the influence of these factors, various metal frames may emerge, differing in the size of the final metal frame, the inter-layer distance, the lattice, the coordination shape, etc. To date, a limited number of Ni(II)–phosphonate materials have been synthesised either through interactions at room temperature or chemical reactivity at high temperatures (hydrothermal and/or solvothermal conditions) [49].

The organophosphonate ligands presented in this work, are multifunctional binders that bind metalloelements in a variety of ways. The iminodiphosphonate and imino-carboxy-phosphonate ligand bind Ni(II) ions in an octahedral fashion, with each phosphonate group in compounds **1** and **2** being singly deprotonated. The variety of lattices achieved through the interaction of metal ions with such binders is exemplified in both **1** and **2**, given that the iminodiphosphonate ligand is coordinated to Ni(II) ion in a monodentate fashion **1**, whereas the imino-carboxy-phosphonate ligand acts as a chelator in **2**. A reflection of the distinct nature of the arising binary Ni(II)–L interactions due to the nature of the ligand L, is the extended structure of **1**, which is composed of a repeat unit configured by four mononuclear Ni(II) octahedral sites. Therefore, the iminodiphosphonate groups of the H_4IDA2P binders exhibit the role of a linker, bringing four Ni(II) ions in each arising unit. Each such unit is basically a 32-membered ring. Each ring defines the periphery of a large elliptical cavity, with the calculated

dimensions being 8.094 Å (*b* axis) and 13.897 Å (*c* axis). The formulated area of each cavity approaches 88.4 $Å^2$. Furthermore, the height of the void space between contiguous elliptical cavities in the lattice is 7.33 Å (*a* axis), thus leading to a volume of ~648 $Å^3$ for each cavity. Complex **1** is X-ray isomorphous to the already characterized species between Co(II) and H_4IDA2P [23]. In conclusion, the nature of the phosphonate substrate does influence the nature of interactions and the ultimately isolated binary Ni(II)–phosphonate compound.

On the basis of the aforementioned grounds, compounds **1** and **2** exhibit composition (exchangeable water ligands, carboxy-phosphonates, phosphonates) and structural properties that could support chemical reactivity toward other metal ionic species (complexes or clusters) under appropriately configured reaction conditions. To this end, **1** and **2** could serve as viable candidate precursor species that can be used in the synthesis of homometallic or heterometallic Ni(II)-(M)-phosphonate advanced materials of variable nuclearity and physicochemical properties (e.g. magnetic). Research in this direction is currently ongoing in our lab.

4. Conclusions

The pH-specific synthetic chemistry presented in this work led to well-defined binary Ni(II)–organophosphonate species of distinct physical, chemical and structural properties. The collective physicochemical properties of **1** and **2** define the characteristics for which such species could be useful in the synthesis of advanced Ni(II)–(carboxy)phosphonate materials. Moreover, in both complexes, the retention of the octahedral environment around Ni(II), suggests that the particular metal ion could interact aptly, in a unique fashion, with imino-phosphonate ligands, such as imino bis(methylenephosphonic acid) and *N*-(phosphonomethyl) glycine, or similar substrates, such as aminoalkylphosphonate and IDA derivative phosphonate substrates. Given the essentiality of Ni(II) in the biological systems as well as its toxicity potential, the herein presented species reflect the nature of the arising binary interactions in potential participants of variably formulated aqueous Ni(II)–phosphoderivative binary systems. It remains to be seen whether species such as those encountered in **1** and **2** reflect corresponding binary forms of Ni(II) with actual phosphorylated cellular targets (amino acids, peptides, etc.) or organophosphonate drug molecules, further influencing the physiology or toxicity at the cellular level.

Supplementary data

CCDC 722262 and 722263 contain the supplementary crystallographic data for **1** and **2**. These data can be obtained free of charge via http://www.ccdc.cam.ac.uk/conts/retrieving.html, or from the Cambridge Crystallographic Data Centre, 12 Union Road, Cambridge CB2 1EZ, UK; fax: (+44) 1223-336-033; or e-mail: deposit@ccdc.cam.ac.uk.

Acknowledgments

This work was supported by a "PENED" grant co-financed by the EU – European Social Fund (75%) and the Greek Ministry of Development – GSRT (25%).

References

[1] T. Li, W. Zhang, R.Z. Lee, Q. Zhong, Food Chem. 114 (2009) 447.
[2] P. Gikas, J. Hazard. Mater. 159 (2008) 187.
[3] P.A. Olubambi, J.H. Potgieter, L. Cornish, Mater. Design 30 (2009) 1451.
[4] J.M. Ramos, O. Versiane, J. Felcman, C.A.S. Tellez, Spectrochim. Acta A 72 (2009) 182.
[5] Q. Chen, J. Salta, J. Zubieta, Inorg. Chem. 32 (1993) 4485.
[6] E.T. Clarke, P.R. Rudolph, A.E. Martell, A. Clearfield, Inorg. Chim. Acta 164 (1989) 59.
[7] P.R. Rudolph, E.T. Clarke, A.E. Martell, A. Clearfield, J. Coord. Chem. 14 (1985) 139.
[8] B. Bujoli, P. Palvadeau, J. Rouxel, Chem. Mater. 2 (1990) 582.
[9] Y. Zhang, A. Clearfield, Inorg. Chem. 31 (1992) 2821.
[10] G. Huan, A.J. Jacobson, J.W. Johnson, E.W. Corcoran Jr., Chem. Mater. 2 (1990) 91.
[11] D.A. Burwell, K.G. Valentine, J.H. Timmermans, M.E. Thompson, J. Am. Chem. Soc. 114 (1992) 4144.
[12] G.L. Rosenthal, J. Caruso, Inorg. Chem. 31 (1992) 3104.
[13] M.B. Dines, P.C. Griffith, Inorg. Chem. 22 (1983) 567.
[14] M.B. Dines, P.M. DiGiacomo, Inorg. Chem. 20 (1981) 92.
[15] H. Byrd, J.K. Pike, D.R. Talham, J. Am. Chem. Soc. 116 (1994) 7903.
[16] R.G.G. Russell, M.J. Rogers, Bone 25 (1999) 97.
[17] O. Bijvoet, H. Fleisch, R.E. Canfield, R.G.G. Russell, in: Bisphosphonates on Bone, Elsevier, Amsterdam, 1995, p. 1.
[18] CrysAlis CCD, Oxford Diffraction Ltd., Version 1.171.29.9, Release 23.03.06.
[19] CrysAlis.NET, CrysAlis RED, Oxford Diffraction Ltd., Version 1.171.29.9, Release 23.03.06.
[20] G.M. Sheldrick, SHELX-97: Program for the Solution of Crystal Structure, University of Göttingen, Göttingen, Germany, 1997.
[21] G.M. Sheldrick, SHELX-97: Program for the Refinement of Crystal Structure, University of Göttingen, Göttingen, Germany, 1993-7, Release 97-2.
[22] L.J. Farrugia, J. Appl. Cryst. 32 (1999) 837.
[23] H. Jankovics, M. Daskalakis, C.P. Raptopoulou, A. Terzis, V. Tangoulis, J. Giapintzakis, T. Kiss, A. Salifoglou, Inorg. Chem. 41 (2002) 3366.
[24] D. Kong, Y. Li, X. Ouyang, A.V. Prosvirin, H. Zhao, J.H. Ross, K.R. Dunbar, A. Clearfield, Chem. Mater. 16 (2004) 3020.
[25] B.-P. Yang, A.V. Prosvirin, H.-H. Zhao, J.-G. Mao, J. Solid State Chem. 179 (2006) 175.
[26] B.-P. Yang, Z.-M. Sun, J.-G. Mao, Inorg. Chim. Acta 357 (2004) 1583.
[27] B.-P. Yang, J.-G. Mao, Inorg. Chem. 44 (2005) 566.
[28] J.-L. Song, J.-G. Mao, Y.-Q. Sun, H.-Y. Zeng, R.K. Kremer, A. Clearfield, J. Solid State Chem. 177 (2004) 633.
[29] J.G. Mao, Z. Wang, A. Clearfield, J. Chem. Soc., Dalton Trans. 24 (2002) 4541.
[30] D. Kong, J. Reibenspies, J. Mao, A. Clearfield, A.E. Martell, Inorg. Chim. Acta 342 (2003) 158.
[31] F.-N. Shi, F.A.A. Paza, P.I. Girginova, L. Mafra, V.S. Amaral, J. Rocha, A. Makal, K. Wozniak, J. Klinowski, T. Trindade, J. Mol. Struct. 754 (2005) 51.
[32] V.S. Sergienko, G.G. Aleksandrov, E.G. Afonin, Zh. Neorg. Khim. 42 (1997) 1291.
[33] V.S. Sergienko, E.G. Afonin, G.G. Aleksandrov, Zh. Neorg. Khim. 43 (1998) 1002.
[34] Y.Q. Zheng, Z.P. Kong, J. Coord. Chem. 56 (2003) 967.
[35] H. Aghabozorg, R.C. Palenik, G.J. Palenik, Inorg. Chem. 24 (1985) 4216.
[36] T.-T. Pan, J.-R. Su, D.-J. Xu, Acta Cryst. E61 (2005) m1376.
[37] E.E. Sileoa, A.S. Araujob, G. Rigottic, O.E. Piroc, E.E. Castellano, J. Mol. Struct. 644 (2003) 67.
[38] Q.-J. Deng, M.-H. Zeng, H. Liang, K.-L. Huang, Acta Cryst. C62 (2006) m389.
[39] N. Stock, Solid State. Sci. 4 (2002) 1089.
[40] D. Heineke, S.J. Franklin, K.N. Raymond, Inorg. Chem. 33 (1994) 2413.
[41] E. Galdecka, Z. Galdecki, P. Gawryszewska, J. Legendziewicz, New J. Chem. 24 (2000) 387.
[42] R.S. Drago, in: Physical Methods in Chemistry, W.B. Saunders Company, Philadelphia, 1977, pp. 359–410.
[43] A.B.P. Lever, in: Inorganic Electronic Spectroscopy, second ed., Elsevier, Amsterdam, 1984, pp. 507–511.
[44] M. Ramstedt, C. Norgren, J. Sheals, D. Boström, S. Sjöberg, P. Persson, Inorg. Chim. Acta 357 (2004) 1185.
[45] G. Cao, V.M. Lynch, J.S. Swinnea, T.E. Mallouk, Inorg. Chem. 29 (1990) 2112.
[46] G.B. Hix, V.J. Carter, D.S. Wragg, R.E. Morris, P.A. Wright, J. Mater. Chem. 9 (1999) 179.
[47] S. Drumel, P. Janvier, P. Barboux, M. Bujoli-Doeuff, B. Bujoli, Inorg. Chem. 34 (1995) 148.
[48] S. Drumel, P. Janvier, P. Barboux, M. Bujoli-Doeuff, B. Bujoli, New J. Chem. 19 (1995) 239.
[49] B. Menaa, I.J. Shannon, J. Mater. 12 (2002) 350.